Near-surface *in vitro* studies of plasma sprayed hydroxyapatite coatings

T. P. Ntsoane[a)]
Research and Development Division, NECSA Limited, P.O. Box 582, Pretoria, 0001, South Africa

M. Topic and R. Bucher
Department of Materials Research, iThemba Laboratory, P.O. Box 722, Somerset West, 7129, South Africa

(Received 22 February 2011; accepted 2 March 2011)

Coatings of plasma sprayed hydroxyapatite (HAp), incubated in simulated body fluid for periods varying from 1 to 56 days, were characterized using conventional laboratory X rays. Quantitative phase analysis, employing TOPAS software, showed an opposite trend in the two main phases of the coating, viz., HAp and tetracalcium phosphate (TTCP). The former increased within the first 7 days of incubation whilst the latter decreased during the same period; both phases stabilized with further incubation. The crystallinity of the coatings exhibited a trend similar to that of HAp i.e., an increase in the early stages of incubation stabilization with further incubation. Results of residual stress determined with Bruker's D8 Discover and analyzed with LEPTOS software, showed both the normal stress tensor components, σ_{11} and σ_{22}, to be tensile, relaxing significantly in the early stages of incubation before stabilizing with further incubation. © *2011 International Centre for Diffraction Data.* [DOI: 10.1154/1.3583181]

Key words: X-ray diffraction, quantitative phase analysis, Rietveld refinement, residual stress

I. INTRODUCTION

Hydroxyapatite (HAp, $Ca_{10}(PO_4)_6OH_2$), due to its similarity to the mineral component of the bone, is widely used in biomedical applications. Applications range from artificial eye (Colen, 2000) in non-load-bearing to hip and dental implants (Geesink *et al.*, 1987) for improved biological fixation in load-bearing application. However, its poor mechanical properties, such as its brittleness, limits bulk utilization of HAp in the latter. In such applications, the material is rather applied as a coating on metallic substrates such as Ti, Ti alloy, and Cr, thereby combining the excellent mechanical properties of the metal with the osse-integration ability of the bioactive material (de Groot *et al.*, 1987). Thermal spraying, due to a number of advantages, is often the technique of choice in depositing the coating to the substrate. The high temperature present in the plasma melts and thermally decomposes the powder (Yang *et al.*, 1995), resulting in reduced crystallinity (Gross *et al.*, 1998) and undesirable metastable phases (Gross and Berndt, 1998). The latter includes such phases as tricalcium phosphate (TCP), tetracalcium phosphate (TTCP), and calcium oxide. These phases have shown to be more soluble in simulated body fluids (Ducheyne *et al.*, 1993) and hence may compromise the stability and integrity of the coating (Klein *et al.*, 1994). Additionally, differences in thermal expansion coefficients of the coating and substrate materials can lead to the development of residual stresses on cooling (Matejicek *et al.*, 1999). Although a significantly biological performance has been achieved (Habibovic *et al.*, 2005), problems regarding long-term mechanical stability still persists. In this work, laboratory X rays, having shallow penetration depth, were employed for near-surface studies of changes in phase composition, crystallinity, and residual stress induced by spraying as well as the subsequent incubation process. The possible interplay between these factors was also investigated.

II. EXPERIMENTAL METHODS

A. Sample preparation

Hydroxyapatite powder (CAPTAL 90 batch P215), with a size distribution of 120 ± 20 μm, was plasma sprayed onto medical grade Ti–6Al–4V alloy supplied by Biomaterials Limited, North Yorkshire, UK. The powder was supplied by Plasma Biotal Ltd., Tideswell, UK. Disks of 5 mm thickness cut from a 20 mm diameter rod were grit blasted with alumina particles of irregular shape with sizes ranging between 0.5 and 1 mm for improved adhesion. The substrates were then cleaned ultrasonically for 10 min in 10% Tickopur solution mixed with de-ionized water at a temperature of approximately 40 °C. Grain morphology was irregular in shape as shown by electron micrograph in Figure 1(a).

A closer examination shows that the grains are a conglomerate of small crystals. Hence, they have a porous microstructure [see Figure 1(b)]. Plasma spraying of the substrates was done under atmospheric conditions using a PT M-1000 system equipped with a Sulzer Metco F4 MB plasmatron. The desired plasma heating was provided by a mixture of hydrogen and argon gases. The latter was also used as the carrier gas to transport the powder into the plasma. No external medium was applied to the coating-substrate system for cooling. The powder was injected externally into the plasma following the normal direction of the plasma plume axis. Details of the coating parameters are shown in Table I.

B. Incubation experiment

To mimic *in vivo* changes induced within the physiological environment, the as-sprayed samples were immersed in revised simulated body fluid (rSBF). The solution was based

a)Author to whom correspondence should be addressed. Electronic mail: tshepo.ntsoane@necsa.co.za

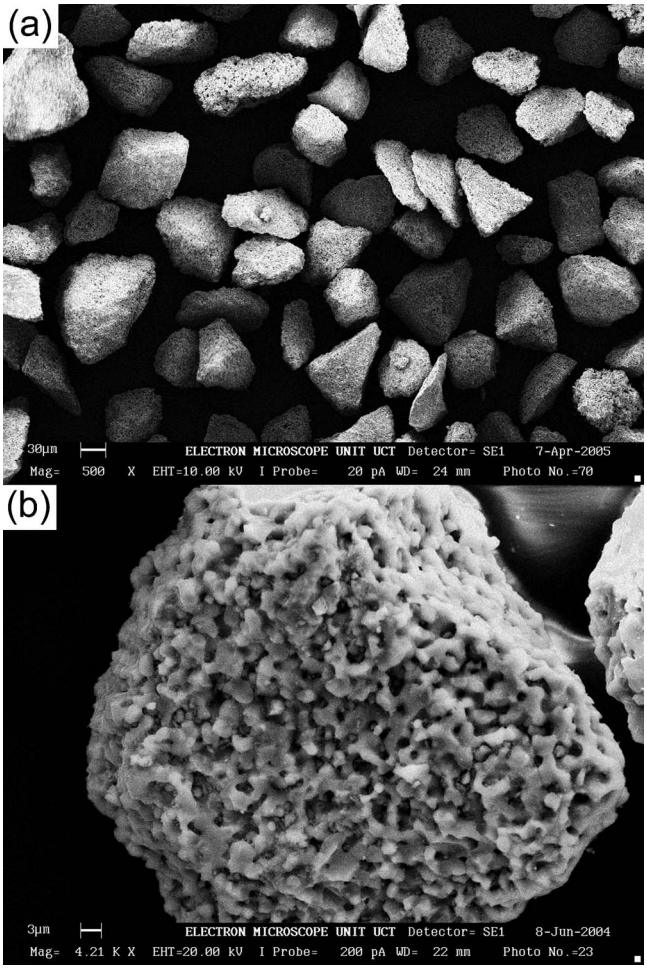

Figure 1. Scanning electron microscopy of the starting hydroxyapatite powder: (a) normal magnification and (b) high magnification showing porous nature of the individual particles.

on Kokubo's formulation (Kokubo *et al.*, 1990) consisting of different amounts of salts in de-ionized water. Compared to human blood plasma, it has a similar ionic concentration but is protein and enzyme free. During the incubation experiment, the temperature and *p*H of the solution were kept at 36 °C and 7.4, respectively. Monitoring of the *p*H was done electronically with adjustment carried out by adding NaOH. The solution was continuously stirred to avoid any formation and build-up of precipitates. The samples were placed in an incubator maintained at 36 ± 1 °C for periods of 1, 7, 28, and 56 days. The volume $V(l)$ of the rSBF used for incubating the samples was calculated as follows:

$$V = \frac{A}{3.33\ \mathrm{m}^{-3}}, \tag{1}$$

where A is the coated area to be immersed in the solution. After incubation, the samples were rinsed with de-ionized water and dried at 100 °C for 24 h.

TABLE I. Parameters used in the plasma spray of Ti–6Al–4V substrate.

Parameter	Value
Primary plasma gas (Slpm)	45
Secondary plasma gas (Slpm)	6.5
Carrier gas (Slpm)	5
Relative powder feed rate (%)	20
Relative hopper stirrer rate (%)	40
Spray distance (mm)	90
Plasma power (kW)	30
Horizontal speed (m/s)	0.1
Traverse speed (m/s)	0.017

TABLE II. D8 Advance measurement details of the sprayed and incubated coatings.

Parameter	Value
Wavelength (Å)	1.5406
2θ scan range (deg)	55
Step size (deg)	0.02
Counting time per step (s)	0.4
Current (mA)	40
Voltage (kV)	40
Mean temperature (°C)	21

1. Morphology and phase identification

The morphology of the starting powder and deposited layers were investigated by scanning electron microscopy. Phase identification was carried out using X-ray diffractometry techniques. Measurements were carried out on a Bruker D8 Advance diffractometer operated in parallel beam geometry. Probing was done using the 8 keV Cu $K\alpha$ radiations with the scattered beam collected using a Lynx eye detector. Details of the measurement parameters are shown in Table II.

Analysis of data for qualitative and quantitative phase identification was done using both Bruker (2007) EVA v13 (Diffrac^{plus}) and TOPAS v4.2 (Coelho, 2007) softwares, respectively. The latter employed Rietveld refinement with the starting structure files supplied by the manufacturer's database and was also utilized for crystallinity examination.

2. Strain determination

The effect of stress on a polycrystalline sample is a change in the lattice spacing of the diffracting lattice planes, which in 0D and 1D diffractometry is characterized by a shift in the corresponding diffraction peak position. In 2D X-ray diffraction (2D XRD), the presence of residual stresses is indicated by the distortion of the corresponding Debye rings. The theory of stress determination employing 2D XRD is well documented (He *et al.*, 2000). The strain tensor, ε_{ij}, determined in the sample coordinate system $S_1S_2S_3$, with sample orientation (ω, ϕ, ψ), and distortion of the diffraction ring in a particular direction $(\eta, 2\theta)$ are related by

$$f_{11}\cdot\varepsilon_{11} + f_{12}\cdot\varepsilon_{12} + f_{22}\cdot\varepsilon_{22} + f_{13}\cdot\varepsilon_{13} + f_{23}\cdot\varepsilon_{23} + f_{33}\cdot\varepsilon_{33} = \ln\left(\frac{\sin\theta_0}{\sin\theta}\right), \tag{2}$$

where f_{ij} are the strain coefficients, $\ln(\sin\theta_0/\sin\theta)$ is the diffraction cone distortion for a particular $(\eta, 2\theta)$ position, and θ_0 is the peak position for a stress-free material. The strain tensor components can then be determined by least-squares fitting of Eq. (2). Using Hooke's law and assum-

https://doi.org/10.1154/1.3583181 Published online by Cambridge University Press

ing isotropic conditions, the above equation can be expressed in terms of the stress tensor components as

$$p_{11}\sigma_{11} + p_{12}\sigma_{12} + p_{13}\sigma_{13} + p_{22}\sigma_{22} + p_{23}\sigma_{23} + p_{33}\sigma_{33} = \ln\left(\frac{\sin\theta_0}{\sin\theta}\right), \quad (3)$$

where p_{ij} are constants. The above equation can be reduced further in the case of a biaxial stress state. Strain measurements were carried out on a Bruker D8 Discover X-ray diffractometer. The beam optics included a graphite monochromator and a 0.8 mm diameter collimator on the primary side, while the diffracted beam was collected using a High Star two-dimensional detector. A laser-video alignment system, with an accuracy of ~ 20 μm, was used for sample positioning. Measurements were performed with Cu $K\alpha$ radiation in side-inclination mode (Noyan and Cohen, 1987). Due to shielding of the detector at high sample tilt angles, measurements were limited to maximum tilt angle of 77° in 2θ.

The diffraction data were analyzed using Bruker (2008) LEPTOS software (Diffrac^{plus}). The software first bins the Debye ring into slices of required width and thickness. The sliced data are then reduced into Cartesian format and η-integrated into 1D diffraction profiles. The profile peaks are then fitted with a function of choice such as parabolic, PV, etc., for the determination of peak position. The calculated peak positions from the previous step are then used in least-squares fitting of Eq. (2) for the determination of tensor components.

III. RESULTS AND DISCUSSION

Figure 2 shows the electron micrograph of the as-sprayed and incubated coatings. The as-sprayed coating surface has a typical plasma sprayed morphology characterized by glassy regions, resulting from the complete flattening and quenching of molten particles [see Figure 2(a)]. Partially molten and unmolten particles, in the form of hemispheres, can be seen scattered across the surface. Cracks, suggesting the presence of residual stresses, can also be seen running across the surface. Within the first 7 days of incubation, the surface indicated an increased roughness [see Figure 2(b)], with the partially molten and unmolten particles as well as the glassy regions disappearing. This is due to the dissolution of loosely bound particles and thermally decomposed phases.

Upon closer examination, the onset of small spherical precipitates, as indicated by a black circle in Figure 2(b), can be seen across the surface. The continued dissolution enlarges the initial pore size to a large open volume as indicated by white circles. Surface morphology of the coating incubated for 28 days is shown in Figure 2(c). From the figure, it can be seen that with further immersion time, the precipitates increase in both number and size covering a bigger surface area as illustrated by the black circle. In addition to the increase in size and number of precipitates, thin needle-shaped fibers start to appear (see the white circles). After 56 days of incubation, the coating shows more and more surface being covered by a precipitate layer, as shown in Figure 2(d). TEM studies previously done by other authors (Lu and Leng, 2004) have identified the precipitates as octacalcium phosphate.

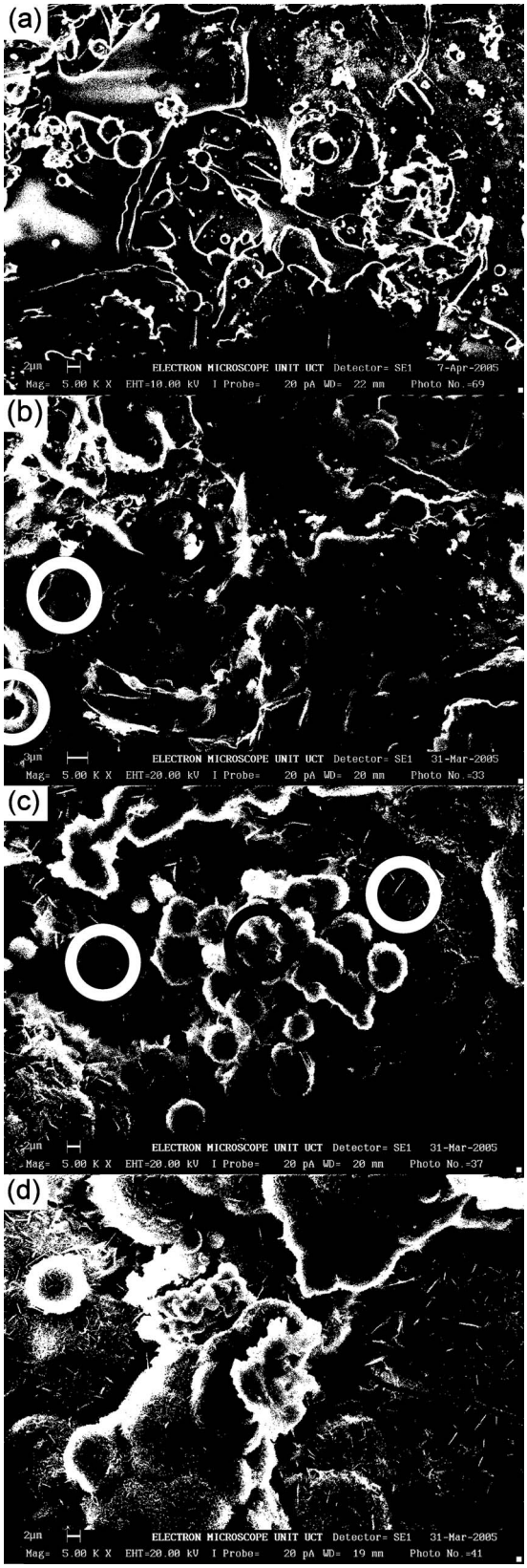

Figure 2. Scanning electron micrograph of the as-sprayed and immersed coatings: (a) as sprayed, (b) 7 days, (c) 28 days, and (d) 56 days incubated.

https://doi.org/10.1154/1.3583181 Published online by Cambridge University Press

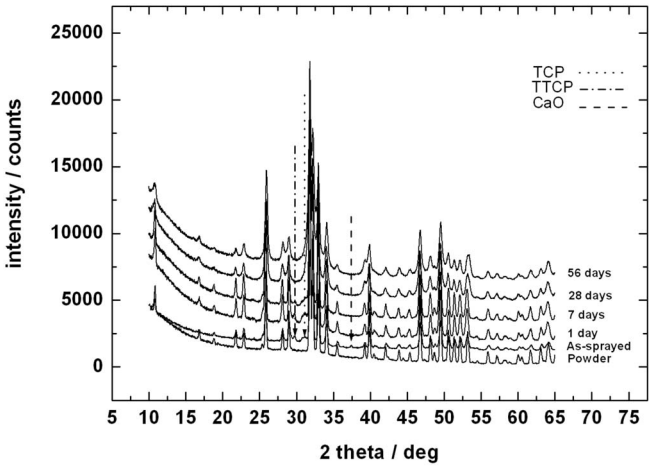

Figure 3. Superposed powder diffraction pattern of HAp coatings exposed to incubation for different periods.

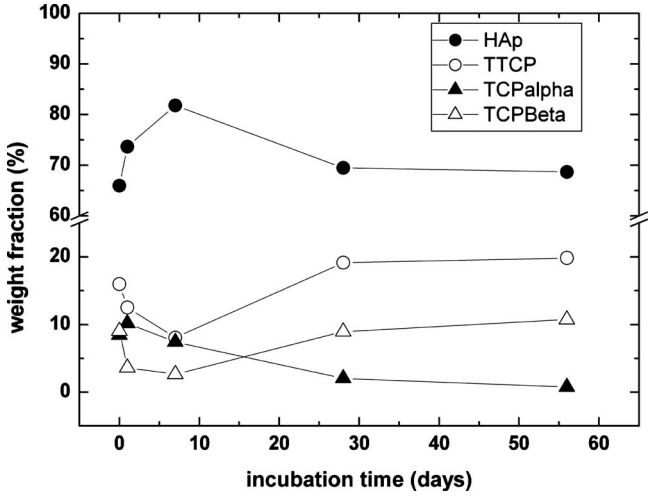

Figure 4. Phase distribution of HAp with incubation time.

A. Powder diffraction

The X-ray diffraction patterns of the HAp powder superimposed on the as-sprayed HAp and incubated coatings are shown in Figure 3. The patterns show that in addition to the initial HAp phase, new phases with corresponding peaks at 2θ positions ~29°, 30°, and 37° can be seen in the figure. Previous work by other authors have identified as the phases as TTCP, TCP, and CaO, resulting from thermal decomposition. It can be seen that, within the first day of incubation, the calcium oxide peak at ~37° 2θ has disappeared, while a decrease in the intensity of the tricalcium phosphate and tetracalcium phosphate peaks, indicated by the solid and dashed arrows in the figure, is noticeable.

For an incubation period of seven days, the tricalcium phosphate can barely be seen whilst the calcium oxide peak has completely disappeared and the TTCP peaks are still visible. This is in agreement with Chern Lin *et al.* (1994), who showed that most impurities disappear within the first 10 days. With further incubation, the peak intensity of HAp continues to decrease, as can be seen in the pattern of the 28 days incubated sample. After 56 days of further incubation, all the thermally decomposed peaks have significantly disappeared. An increasing peak broadening, more pronounced at high 2θ around 90°, leads to fusing of overlapping peaks, as shown in the patterns of the 28 and 56 day incubated samples. The weight fractions of the different phases, determined using TOPAS v4 at various stages of incubation, are presented in Figure 4. The figure shows that, in all incubation stages, HAp remains the main phase.

The two major phases, HAp and TTCP, show an opposite trend. In the former, the weight percent increases from $65.94 \pm 0.4\%$ to $81.83 \pm 0.33\%$ within the first 7 days followed by a gradual decrease before saturating at ~69%. On the other hand, TTCP decreases from ~16% to ~8.0% in the same period followed by a dramatic increase before saturation around 19%. The apparent increase in HAp after 7 days of incubation is due to dissolution of the thermally decomposed phases leaving behind the more stable HAp. This is a testimony to Radin and Ducheyne (1992), whose studies have shown that the thermally decomposed products dissolve faster as compared to the original crystalline HAp. They have also reported nearly two orders of magnitude in dissolution of sprayed coatings as compared to the starting powder. The dissolution rate increases in the following order (Sun *et al.*, 2002):

$$\text{HAp} < \text{CaO} < \beta\text{-TCP} < \alpha\text{-TCP} < \text{TTCP} < \text{ACP} < \text{DCP}. \quad (4)$$

The acronyms ACP and DCP refer to amorphous calcium phosphate and dicalcium phosphate, respectively. The reduction in HAp observed at intermediate periods can be attributed either to an increased dissolution of HAp after the 7 days, which according to Eq. (4) is not possible, or the existence of a phase composition gradient within the coating thickness. The latter is most likely the case as a result of a possible temperature gradient created during spraying. Such a gradient will have implications on the phase composition of the coating. The dissolution of the outer regions of the coating will expose such a depth dependence of the phase as it removes these regions of the coating. However, Fazan and Marquis (2000) showed that the dissolution process does not continue monotonically with incubation time. At some point, a maximum is reached from which it starts declining or remains constant. A saturated solution nucleates and precipitates, forming bonelike apatite nanocrystals on the coating surface, as shown in Figs. 4(c) and 4(d). This has a "shielding" effect on the dissolving ions, reducing or inhibiting further dissolution, as illustrated by the stabilization of both phases at longer immersion periods i.e., from 28 days onwards.

B. Crystallinity

Figure 5 shows the variation of crystallinity with incubation time. The as-received powder showed crystalline of 99.85%, which upon spraying became slightly amorphous at 90.5%. This is attributed to a quenching effect of the molten splat whereby the individual atoms or molecules are "frozen" on impact inhibiting their rearrangement into a crystalline pattern. As with HAp weight fraction, the crystallinity increases from 90.5% to maximum of ~98% within the first 7 days, before decreasing and stabilizing at 81% at 56 days of incubation. Amorphous calcium phosphate, being one of the

https://doi.org/10.1154/1.3583181 Published online by Cambridge University Press

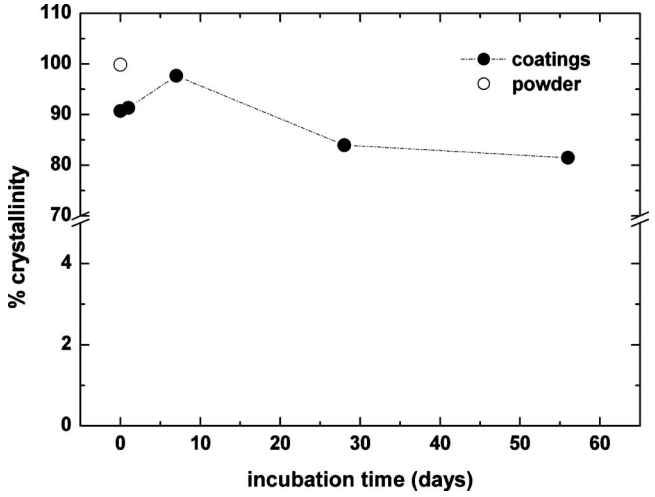

Figure 5. Variation of degree of crystallinity with incubation time.

more soluble phases, dissolves quickly leaving behind a more crystalline coating. Again the behavior of the pattern follows the same explanation as that of phase composition.

C. Residual stress

Figure 6 shows the normal residual stress tensor of HAp coating incubated for varying times. The stress tensor components were calculated using X-ray elastic constants of hydroxyapatite, $S_1 = -2.48 \times 10^{-6}$ MPa^{-1} and $1/2S_2 = 11.5 \times 10^{-6}$ MPa^{-1}(Nye, 1957) for the 213 reflections. The Kroner–Eshelby interaction model was assumed in the calculations.

Both the normal tensor components (σ_{11} and σ_{22}) are tensile for the as-sprayed coating, decreasing from 135 to 30 MPa and 79 to 40 MPa, respectively. The shear components showed negligible stresses. Yang *et al.* (2003), performing similar investigations on rectangular samples, recorded a compressive surface stress of 44 MPa in the as-sprayed coating, relaxing to 21.2 MPa after 28 days of incubation. The theoretically expected tensile stresses in the as-sprayed coating have also been reported by other authors. Both Brown *et al.* (1994) and Sergo *et al.* (1997), although employing different techniques, recorded the tensile stresses. The observed relaxation of the normal stresses can be attributed to an increase in porosity density as well as open volume defects resulting from dissolution.

IV. CONCLUSION

Near-surface *in vitro* studies of HAp coatings, for penetration depth <10 μm, were carried out using X-ray diffractometry. Results showed that the first 7 days of coating immersion are crucial for the dissolution of thermally decomposed products and amorphous phase as illustrated by significant changes in phase composition and coating crystallinity. The intermediate period showed solution precipitation on the surface dominating, thereby "shielding" the underlying coating from further dissolution. Dissolution of the soluble phases in the early stages of incubation relaxed the normal residual stress components, σ_{11} and σ_{22}, before stabilizing at longer immersion periods.

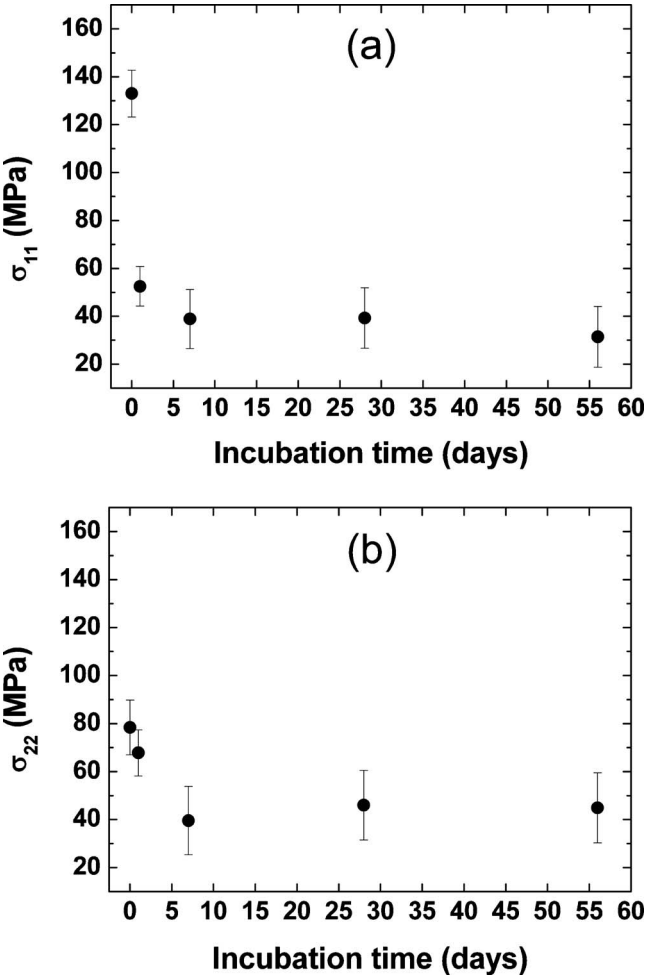

Figure 6. Variation of normal residual stress tensor of HAp coatings with incubation: (a) σ_{11} and (b) σ_{22}.

ACKNOWLEDGMENTS

The authors are indebted to Margitta Hengst, Department of Mineralogy, Technische Universität Bergakademie, Freiberg, Germany for providing the samples. The work was sponsored by the German Federal Ministry of Research and Technology (BMBF) and National Research Foundation of the Republic South Africa within the research project "Characterisation and determination of residual stress in bioactive coatings and layered structure" Project Code No. 39.6.G0B.6.A.

Brown, S. R., Turner, I. G., and Reiter, H. (**1994**). "Residual stress measurement in thermal sprayed hydroxyapatite coatings," J. Mater. Sci. Mater. Med. **5**, 756–759.

Bruker (**2007**). Diffrac^{plus} Basic Evaluation Package (Computer Software) Karlsruhe, Germany.

Bruker (**2008**). Diffrac^{plus} LEPTOS v6 (Computer Software) Karlsruhe, Germany.

Chern Lin, J. H., Liu, M. L., and Ju, C. P. (**1994**). "Morphologic variation in plasma-sprayed hydroxyapatite-bioactive glass composite coating in Hank's solution," J. Biomed. Mater. Res. **28**, 273–730.

Coelho, A. A. (**2007**). TOPAS-ACADEMIC, version 4.1 (Computer Software), Coelho Software, Brisbane, Australia.

Colen, T. (**2000**). "Comparison of artificial eye amplitudes with acrylic and hydroxyapatite spherical enucleation implants," Ophthalmology (Philadelphia) **107**, 1889–1894.

de Groot, K., Geesink, R., Klein, C. P. A. T., and Serekian, P. (**1987**). "Plasma sprayed coatings of hydroxylapatite," J. Biomed. Mater. Res.

21, 1375–1381.
Ducheyne, P., Radin, S., and King, L. (**1993**). "The effect of calcium phosphate ceramic composition and structure on in vitro behavior. I. Dissolution," J. Biomed. Mater. Res. **27**, 25–34.
Fazan, F., and Marquis, P. M. (**2000**). "Dissolution behavior of plasma-sprayed hydroxyapatite coatings," J. Mater. Sci. Mater. Med. **11**, 787–792.
Geesink, R. G. T., de Groot, K., and Klein, C. P. A. T. (**1987**). "Chemical implant fixation using hydroxyl-apatite coatings: The development of a human total hip prothesis for chemical fixation to bone using hydroxyl-apatite coatings on titanium substrates," Clin. Orthop. Relat. Res. **225**, 147–170.
Gross, K. A., Benrdt, C. C., and Herman, H. (**1998**). "Amorphous phase formation in plasma-sprayed hydroxyapatite coatings," J. Biomed. Mater. Res. **39**, 407–414.
Gross, K. A., and Berndt, C. C. (**1998**). "Thermal processing of hydroapatite for coating production," J. Biomed. Mater. Res. **39**, 580–587.
Habibovic, P., Li, J., van der Valk, C. M., Meijer, G., Layrolle, P., van Blitterswijk, C. A., and de Groot, K. (**2005**). "Biological performance of uncoated and octacalcium phosphate- coated Ti6Al4V," Biomaterials **26**, 23–36.
He, B. B., Preckwinkel, U., and Smith, K. L. (**2000**). "Fundamentals of two-dimensional X-ray diffraction (XRD^2)," Adv. X-Ray Anal. **43**, 273–280.
Klein, C. P. A. T., Patka, P., Wolke, J. G. C., de Bliek-Hogervorst, J. M. A., and de Groot, K. (**1994**). "Long term in vivo study of plasma sprayed coatings on titanium alloy of tetra calcium phosphate, hydroxyapatite and alpha tricalcium phosphate," Biomaterials **15**, 146–150.
Kokubo, T., Kushitani, H., Sakka, S., Kitsugi, T., and Yamamuro, T. (**1990**). "Solutions able to reproduce in vivo surface-structure changes in bioactive glass-ceramic A-W," J. Biomed. Mater. Res. **24**, 721–734.
Lu, X., and Leng, Y. (**2004**). "TEM study of calcium phosphate precipitation on bioactive titanium surfaces," Biomaterials **25**, 1779–1786.
Matejicek, J., Sampath, S., Brand, P. C., and Prask, H. (**1999**). "Quenching, thermal and residual stress in plasma sprayed deposits: NiCrAlY and YSZ coatings," Acta Metall. **47**, 607–617.
Noyan, I. C., and Cohen, J. B. (**1987**). *Residual Stress Measurement by Diffraction and Interpretation* (Springer-Verlag, New York).
Nye, J. F. (**1957**). *Physical Properties of Crystal* (Clarendon, Oxford).
Radin, S. R., and Ducheyne, P. (**1992**). "Plasma spraying induced changes of calcium phosphate ceramic characteristics and the effect on in vitro stability," J. Mater. Sci.: Mater. Med. **3**, 33–42.
Sergo, V., Sbaizero, O., and Clarke, D. R. (**1997**). "Mechanical and chemical consequences of the residual stresses in plasma sprayed hydroxyapatite coatings," Biomaterials **18**, 477–482.
Sun, L., Berndt, C. C., Khor, K. A., Cheang, H. N., and Gross, K. A. (**2002**). "Surface characteristics and dissolution behavior of plasma-sprayed hydroxyapatite coating," J. Biomed. Mater. Res. **62**, 228–236.
Yang, C. Y., Wang, B. C., Chang, E., and Wu, J. D. (**1995**). "The influence of plasma spraying parameters on the characteristics of hydroxyapatite coatings: A quantitative study," J. Mater. Sci.: Mater. Med. **6**, 249–257.
Yang, Y. C., Chang, E., and Lee, S. Y. (**2003**). ""Mechanical properties and Young's modulus of plasma-sprayed hydroxyapatite coating on Ti substrate in simulated body fluid," J. Biomed. Mater. Res. Part A **67**, 886–899.